Journal of Applied Fluid Mechanics, Vol. 17, No. 11, pp. 2390-2400, 2024.
Available online at www.jafmonline.net, ISSN 1735-3572, EISSN 1735-3645.
https://doi.org/10.47176/jafm.17.11.2563

Enhancing Aerodynamic Performance of Double Rectangular Cylinders through Numerical Analysis at Varying Inclinations

S. Chamoli[1], A. Phila[2], P. Sanwal[1], H. Adhikari[1], H. Rana[1], P. Pant[1], A. Joshi[1], C. Thianpong[3] and S. Eiamsa-ard[2†]

[1] *Department of Mechanical Engineering, Govind Ballabh Pant Institute of Engineering & Technology, Pauri Garhwal, Uttarakhand, 246194, India*
[2] *Department of Mechanical Engineering, School of Engineering and Industrial Technology, Mahanakorn University of Technology, Bangkok, 10530, Thailand*
[3] *School of Engineering, King Mongkut's Institute of Technology Ladkrabang, Bangkok, 10520, Thailand*

†*Corresponding Author Email: smith@mut.ac.th*

ABSTRACT

In the present work, numerical simulations are conducted for external flow through a double rectangular cylinder with different inclinations at Reynolds number (*Re*) 50 to 200 based on free stream velocity. The cylinder aspect ratio is considered to be fixed at 0.25. During the numerical simulations, one cylinder is kept fixed, and the other cylinder is inclined at 'θ = 20°' first clockwise and then in an anticlockwise direction alternatively for both cylinders. Because of the inclined cylinder, the vortex dynamics lead to significant changes in flow-induced forces. In this article, the focus is given to how *Re* and inclination in the cylinder influence the flow structures and associated aerodynamic properties. It is shown that when any of the cylinders are inclined, a significant decrease in the average drag coefficient is noticed as compared to the parallel cylinder case. In a similar manner, the lift coefficient also decreases when any one of the cylinders is inclined at θ = 20° either clockwise or counterclockwise as compared to the parallel cylinder case.

Article History

Received January 17, 2024
Revised May 8, 2024
Accepted May 14, 2024
Available online September 1, 2024

Keywords:

Numerical simulation
Lift coefficient
Drag coefficient
Strouhal number
Double rectangular cylinder

1. INTRODUCTION

In the subject of fluid dynamics, fluid flow through a rectangular cylinder is a typical and much-researched phenomenon. Analyzing the flow structures, forces, and thermal properties surrounding a rectangular item exposed to a fluid stream is necessary. Numerous technical specialities, including aerospace, civil engineering, and the automobile industry, use this kind of analysis. A fluid (such as air or water) flows through a rectangular cylinder and interacts with it in a sophisticated way. One of the variables that can change how a flow behaves is *Re*, which is a dimensionless quantity that links the flow's inertial forces to its viscous forces. The flow regime is determined by the Reynolds number, which also has a big impact on the flow characteristics.

The flow through a rectangular cylinder is typically laminar at low *Re*, with smooth and well-organized streamlines. The flow changes to a turbulent phase at higher *Re*, which is characterized by chaotic and erratic flow patterns as the Reynolds number rises. Due to the significance of flow around rectangular cylinders in offshore engineering applications, this topic has received much study. For instance, semi-submersible pontoons and columns of tension-leg platforms.

In a tandem cylinder layout, two cylinders are arranged in a straight line, one after the other, along the flow direction. This shape is frequently used in technical applications such as bluff body aerodynamics, heat exchangers, and aerofoil designs. Below are some earlier studies relevant to this issue. Mashhadi et al. (2021) performed numerical simulations of unconfined flows through rectangular cylinders in two and three dimensions at Reynolds numbers between 30 and 200. The range of the cylinder's cross-sectional aspect ratio, or *L/W*, is 0.25, 0.5, 1.0, 2.0, 3.0, and 4.0. The influence of AR and *Re* on the flow structure and related aerodynamic parameters is highlighted. Sharma and Eswaran (2004) assessed the cross-flow properties and flow structure of a single square cylinder in 2D domain for *Re* ranging from 1.0 to 160 in both steady and unsteady periodic laminar flow. Tian et al. (2013) investigated the flow around rectangular cylinders with various aspect ratios using the *k-ω* shear stress transport turbulence model. The flow separation of an incompressible fluid around a square cylinder was also

NOMENCLATURE

AR	length-to-width aspect ratio	Re	Reynolds number
C_d	time-mean drag coefficient	St	Strouhal number
C_l	lift coefficient	u_{in}	Incoming fluid velocity in x direction
D	width of cylinder cross-section	τ	Time in seconds
f	vortex shedding frequency	W	length of cylinder cross-section
F_d	drag force	μ	dynamic viscosity of the fluid
F_L	lift force	ρ	fluid density

assessed by Jiang and Cheng (2020). Sen et al. (2011) simulated the flow through a stationary square cylinder at zero incidences low *Re* of 150, and the results are given. Using a stable finite-element model, the equations for incompressible fluid flow in two dimensions are discretized. The cylinder with square sections is bluffer than the one with circular sections. Of all the cylinder shapes tested, the square cylinder with sharp corners generates the highest drag. The aim of the study conducted by Khademinezhad et al. (2015) is to investigate the vortex forms and lift and drag coefficients in flows around a square cylinder in contrast to a circular cylinder using the commercial Fluent software. Additionally, the influence of *Re* on the growth of the vortex structures and the velocity field is investigated and contrasted for both circular and square cylinders at different times. Islam et al. (2017) conducted a numerical analysis to use smaller control cylinders upstream/downstream of the main cylinder to prevent vortex shedding and decrease drag trailing a square cylinder. Liu et al. (2019) observed at the flow through two nearby inclined circular cylinders at low *Re*. The primary findings of this investigation are discussed, along with the impact of the inclination angle on the force coefficients and flow field. The inclination angle was shown to have a considerable effect on the instantaneous and mean flow fields. The axial flow pattern is significantly influenced by the inclination angle. Wang et al. (2020) used numerical analysis to examine the flow around two parallel, identical trapezoidal cylinders.

The flow properties of two cylinders put side by side on a free surface were studied in 2019 by Subburaj and Vengadesan. In flows with low Froude numbers and deep submergence, vortex shedding is observed. Short inter-cylinder lengths allow the vortices to synchronize in the two cylinders and shed at a certain distance from the cylinders. Balachandar and Parker (2002) investigated the beginning of the vortex shed in an array of staggered cylinders. It is noteworthy that with extremely high transfer spacing, a crucial *Re* of 46 is regained. After peaking at around 52.5 at $LY = 3$, the critical Reynolds number first rises as the transfer distance between neighbouring circular cylinders reduces and then rapidly falls as *LY* declines. Rahman et al. (2007) utilized the 2-D finite volume technique to investigate the unsteady flow across a circular cylinder. The 2-D finite volume method has been shown to be very efficient in calculating hydrodynamic forces and capturing vortex shedding. Even at very high Re, the method continues to function well without sacrificing accuracy. Tu et al. (2015) examined the vibrations caused by flow across two circular cylinders that are positioned in tandem and are elastically mounted at low *Re* of 160. Abdollahpour et al. (2023) studied the structure of the recirculating flow over the BFS in both laminar and turbulent regimes. Lekkala et al. (2022) studied the flow characteristics of bluff structures at varying geometries. Various flow regimes occur behind the circular cylinder, each of which is influenced by the effects of gap ratio, rotational rate and span-wise length. Hu et al. (2015) investigated a LES of flow across an inclined finite square cylinder and found that the mean drags coefficient of the cylinder dropped as the inclination increased both forward and backwards. Abbasi et al. (2021) utilized the lattice Boltzmann method to simulate the flow through two parallel square cylinders with a flat plate located in their wake at various gap ratios (L/d = 0.5-10) between the cylinders and plate. They determined that the control plate reduces the average drag force to a maximum of 19%. For $L/d > 2.5$, the influence of the control plate on the reduction of fluid forces appears to decrease.

Numerous researchers have examined fluid flow around a variety of forms, including square, rectangular, and circular, according to the extensive literature study that was previously indicated (Sohankar et al., 1997; Rajani et al., 2016; Zhou, 2021; Mashhadi & Sohankar, 2022; Tahir et al., 2023). One arrangement type that has been intensively studied is tandem arrangements. However, no studies on the double rectangular cylinder with varying slopes have been conducted up to this time. It's important to comprehend how the aerodynamic properties of inclined cylinders change since many constructions are inclined. Regarding this, fluid flow over a rectangular double cylinder with cylinders inclined at a 20° angle and Reynolds numbers ranging from 50 to 200 is now being studied. The aspect ratio $AR = W/D$ has a substantial effect on the formation of the hydrodynamic forces and vortex. The present numerical simulations employ an aspect ratio of 0.25. The estimates from the current study may be used to create constructions like bridges, chimneys, towering buildings, phone towers, aeroplanes, offshore structures, and more.

2. COMPUTATIONAL METHODOLOGY

2.1. Computational Methodology and Description of Computational Domain

ANSYS, a computational fluid dynamics (CFD) program, is used in the current study to simulate laminar flow numerically over two rectangular cylinders. The finite volume method (FVM), as implemented in ANSYS, is used to solve the governing equations for the incompressible laminar flow, including the continuity equation and the Navier-Stokes equations. A central differencing scheme for the diffusive terms and a second-

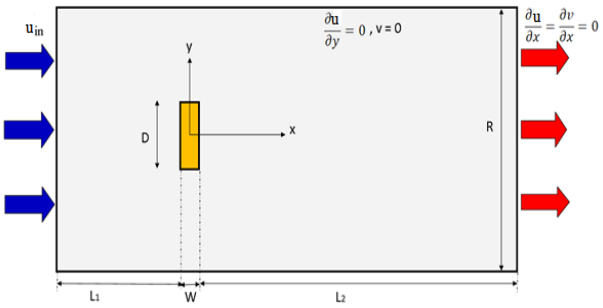

Fig. 1 Computational domain for the flow around a rectangular cylinder used for the code validation and the associated parameter

order upwind scheme for the convective terms are used in the discretization of the governing equations. The SIMPLE algorithm handles the pressure-velocity interaction. There is no use of a turbulence model because the flow is laminar. The next part contains more information on the numerical approach, including the grid independence study and convergence criteria. Figure 1 depicts the computational domain, including the rectangular cylinder. A uniform flow (u_{in}) is applied to the rectangular cylinder. The width and length of the rectangular cylinder's sides are *D* and *W*, respectively. *AR = W/D* is the formula for the aspect ratio of a cylinder's cross-section. The upstream distance $L_1 = 9D$, downstream distance $L_2 = 20D$, and lateral width $R = 18D$ are selected as the computational domain size. The domain is unaffected by obstructions since the distances are suitably large enough.

2.2. Governing Equations

Conservation of mass:

$$\frac{\partial u}{\partial x} + \frac{\partial u}{\partial y} = 0 \tag{1}$$

Conservation of momentum

x-direction:

$$\frac{\partial u}{\partial t} + u\frac{\partial u}{\partial x} + v\frac{\partial u}{\partial x} = -\frac{1}{\rho}\frac{\partial p}{\partial x} + \nu\left(\frac{\partial^2 u}{\partial x^2} + \frac{\partial^2 v}{\partial y^2}\right) \tag{2}$$

y-direction:

$$\frac{\partial v}{\partial t} + u\frac{\partial v}{\partial x} + v\frac{\partial v}{\partial x} = -\frac{1}{\rho}\frac{\partial p}{\partial y} + \nu\left(\frac{\partial^2 u}{\partial x^2} + \frac{\partial^2 v}{\partial y^2}\right) \tag{3}$$

2.3. Parameters

The lift and drag coefficients are calculated as:

$$C_L = C_{LP} + C_{LV} = \frac{F_L}{\frac{1}{2}\rho U_\infty^2 D} \tag{4}$$

$$C_D = C_{DP} + C_{DV} = \frac{F_D}{\frac{1}{2}\rho U_\infty^2 D} \tag{5}$$

The Strouhal number is formed as,

$$St = \frac{FD}{U_\infty} \tag{6}$$

Mathematically, Vorticity is the curl of flow velocity defined as:

$$\vec{\omega} = \nabla \times \vec{u} \tag{7}$$

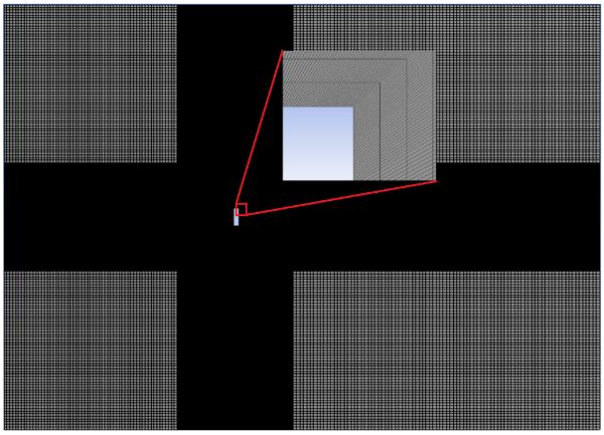

Fig. 2 Code validation computational domain meshing for a single rectangular cylinder

2.4. Meshing and Implemented Boundary Condition in the Computational Domain

Using the commercial software ANSYS, an extremely fine mesh can be implemented in the computational domain. To better capture the vortex shedding behind the cylinders, fine mesh is used around the cylinders, and the mesh size increases from the cylinder surface to the wall boundaries.

In the present case of numerical methodology validation, the mesh has a 1.8 x 10^5 total number of nodes, as presented in Fig. 2. At the entry boundary, a uniform flow velocity is applied corresponding to the flow *Re* from 50 to 200. At the outlet boundary pressure outflow, *i.e.* gauge pressure = 0.0. The top/bottom boundary of the computational domain are taken as symmetry. The detailed implemented boundary condition in the computational domain that is used for code validation is presented in detail in Fig. 2.

2.5. Numerical Methodology Validation

The Strouhal number (*St*) and drag coefficient (C_d) for the uniform flow through an isolated rectangular cylinder are calculated at an aspect ratio of 0.25 in order to validate the numerical methodology used in the current investigation. Validation of data is first performed for transient flow through a rectangular cylinder at *Re* = 150. The geometric and boundary conditions are considered exactly the same as those used by Mashhadi et al. (2021). The average C_d, C_L, and *St* are compared between the present case and by Mashhadi et al. (2021) and presented in Table 1. The percentage of deviation between the present study and Mashhadi et al. (2021) is about 5% or less, which is quite reasonable. Thus, the same numerical methodology is adopted for the present research work of two tandem cylinder arrangements with different inclinations.

2.2 Numerical Settings

After doing numerical methodology validation for a single rectangular cylinder, the current research work, which uses two rectangular tandem cylinders, is considered for numerical calculations. The arrangement is presented in Fig. 3. This representation is of the case

Table 1 Comparison of results for C_d, C_{Lmax}, and *St* obtained with the present numerical method with the data available in the literature

S.no.	Parameter	Present numerical values	Mashhadi et al. [2]
1.	Drag coefficient (C_d)	2.4	2.3235
2.	Maximum Lift coefficient (C_{Lmax})	0.570	0.52710
3.	Strouhal number (*St*)	0.187	0.178

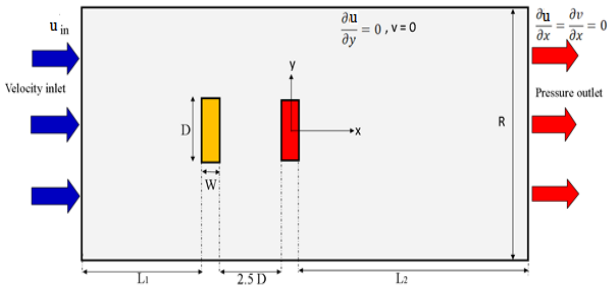

Fig. 3 Computational domain of a rectangular tandem cylinder arrangement with implemented boundary condition

when cylinders are parallel and perpendicular to inlet velocity. The width and length of each rectangular cylinder are *D* and *W*, respectively, and the separation between them is set at 2.5*D*. The computational domain size is set to be the upstream distance L_1 = 10.25 D, downstream distance L_2 = 21.25D, and the lateral width = 21.5*D* in order to reduce the impact of the domain borders on the flow around the cylinder. The implemented boundary condition is the same as the briefly mentioned boundary condition in section 2.1.2 for the numerical simulations of the tandem cylinder configuration.

For analysis of flow structure in rectangular tandem cylinder arrangements, a total of 5 cases are considered and depicted as Case 1 to Case 5 and represented in Fig. 4. Case 1 is considered for the cylinder arrangement when both the cylinders are parallel to each other represented in Fig. 4a. In Case 2 and Case 3, cylinder-1 is fixed, and cylinder-2 is inclined at 20º degrees clockwise and counter-clockwise, respectively and represented in Figs. 4b and 4c, respectively. When cylinder-1 is inclined at 20º degrees counterclockwise, and cylinder-2 is fixed, this arrangement of cylinders is defined as Case 4. A cylinder arrangement in which cylinder-1 is inclined at 20º clockwise, and cylinder-2 is fixed is defined as Case 5.

2.3 Mesh Independency

To check the mesh independency on obtained results from the numerical simulations, two meshes are used. The mesh around the cylinder is taken highly dense with inflation having a growth rate of 1.2, while away from the cylinder, a smaller number of mesh elements are considered. For the meshing of the computational domain, quadrilateral mesh elements are considered with 9.3×10^4 and 1.6×10^5 number of mesh elements for Mesh 1 and 2, as depicted in Fig. 5a and 5b. In Mesh 2, the quadrilateral method has been used by taking the number of divisions between 30 to 200. The cylinder has inflation around its boundaries with 5 layers, a growth rate of 1.2 m and a

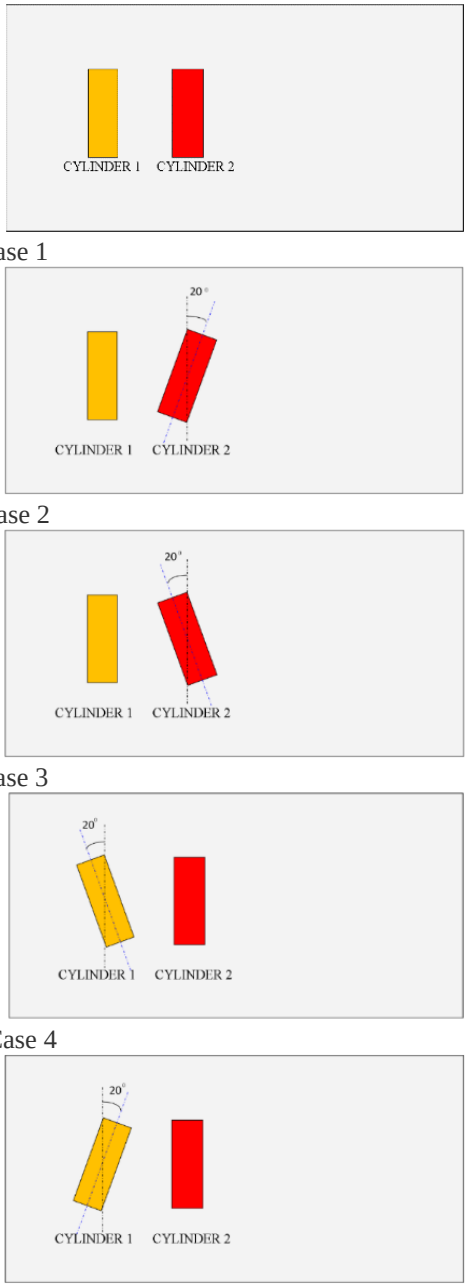

(a) Case 1

(b) Case 2

(c) Case 3

(d) Case 4

(e) Case 5

Fig. 4 Different geometrical considerations for the rectangular cylinders in tandem arrangements: (a) when both the cylinders are parallel to each other, defined as Case 1, (b) when cylinder-1 is fixed, and cylinder-2 is inclined at 20º clockwise and defined as Case 2, (c) when cylinder-1 is fixed, and cylinder-2 is inclined at 20º counter-clockwise and defined as Case 3, (d) when cylinder-1 is inclined at 20º counter-clockwise and cylinder-2 is fixed and defined as Case 4, and (e) when cylinder-1 is inclined at 20º clockwise and cylinder-2 is fixed and defined as Case 5

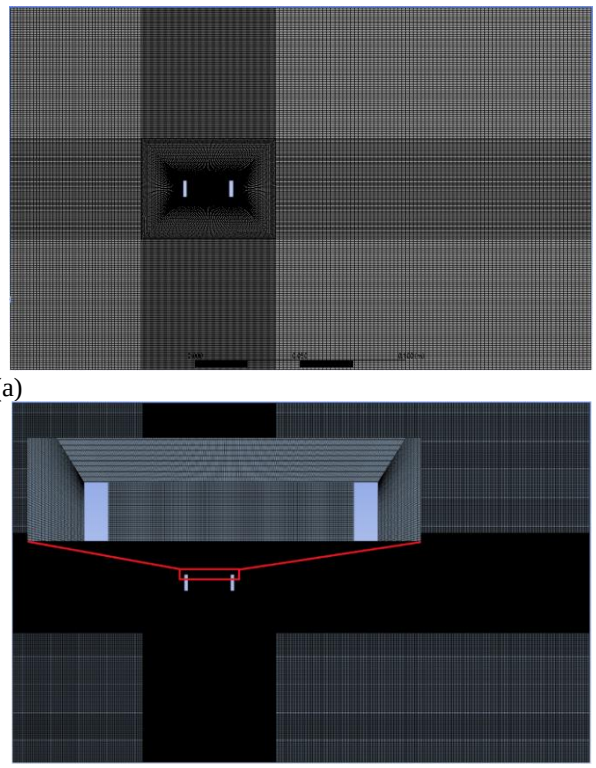

(a)

(b)

Fig. 5 Quadrilateral mesh used in the present computational domain for Case 1, (a) Mesh 1 (Low number of mesh elements), and (b) Mesh 2 (High number of mesh elements)

maximum thickness of 0.1m. The results of the average drag coefficient for Mesh 1 and Mesh 2 are compared and presented in Fig. 6. In the figure, the findings are nearly equal; hence, the results are no longer significantly affected by the number of nodes on the mesh as a result of the results. Furthermore, the *St* number at *Re* = 100 is also compared for Mesh 1 and Mesh 2 and for Cylinder 1 and Cylinder 2 at Mesh 1 and Mesh 2, and the St numbers are 0.0562, 0.0569 and 0.0571, 0.0575, respectively. The change in the *St* number for Mesh 1 and Mesh 2 is less than 2%. As a result, for all numerical simulations, the same set of characteristics and mesh creation approach is used.

3. RESULTS AND DISCUSSION

In this section, instantaneous vorticity contours and instantaneous streamlines for all five cases are presented and discussed.

3.1. Instantaneous Vorticity and Streamlines

The instantaneous vorticity contours and streamlines for are plotted at point A, as mentioned in Fig. 7a, *i.e.* lowest peak point of the lift evolution curve. The local spinning of fluid components in a flow is referred to as vorticity. Due to the existence of the cylinder's surface, vorticity is created when a fluid flows over it. Knowledge of the flow patterns around the cylinder requires a knowledge of the distribution and behavior of vorticity. It provides a useful foundation for comprehending a range of complex flow phenomena, including the formation and

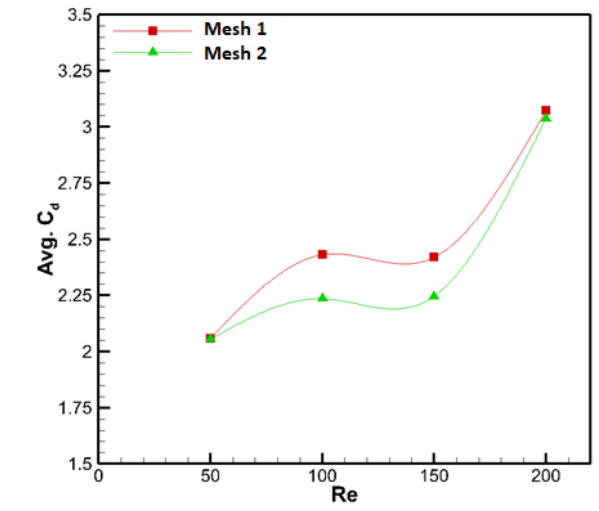

(a)

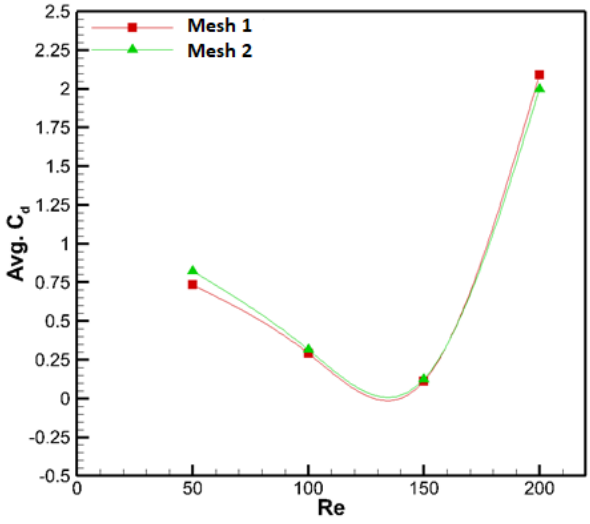

(b)

Fig. 6 Mesh independency test for meshes, *i.e.* Mesh 1 and Mesh for average values of drag coefficient, (a) Cylinder 1, and (b) Cylinder 2

behavior of vortex rings, which makes it a key number in fluid dynamics.

The aforementioned contours in Fig. 7 display the instantaneous vorticity contours at various inclinations illustrated in Cases 1 through 5. Positive and negative vortexes are represented by the hues red and blue. We can tell from the contours that there is excessive complexity in the vortex pattern and strong turbulence close to the cylinder walls. While the positive vortices depicted by the red pattern in the graph arise from the cylinder's bottom wall, the negative vortices depicted by the blue pattern in the graph originate from the top surface. Further investigations show that the vortices in the case of parallel cylinders are more homogeneous and develop more quickly. We see that additional examples, other than the initial cylinder, show strong vorticity. The results demonstrate an increase in the wake length for every inclined cylinder from Case 2 to Case 5. In general, spinning is unexpected when the initial cylinder is inclined, as in Cases 4 and 5. The existence of powerful vortices or share zones is indicated by regions with

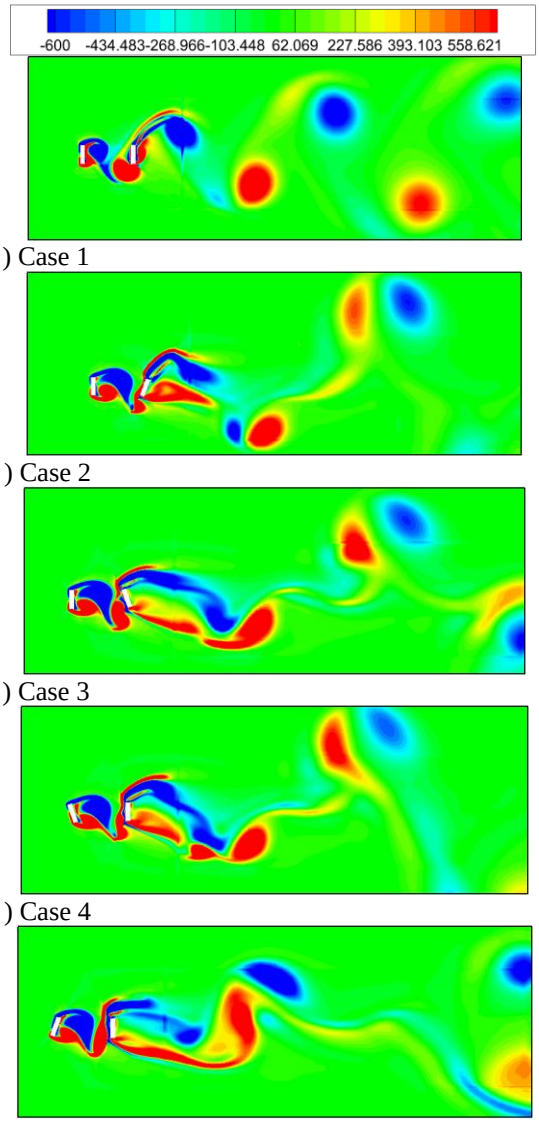

Fig. 7 Instantaneous vorticity contours at the point A, *i.e.* the lowest peak of the lift curve

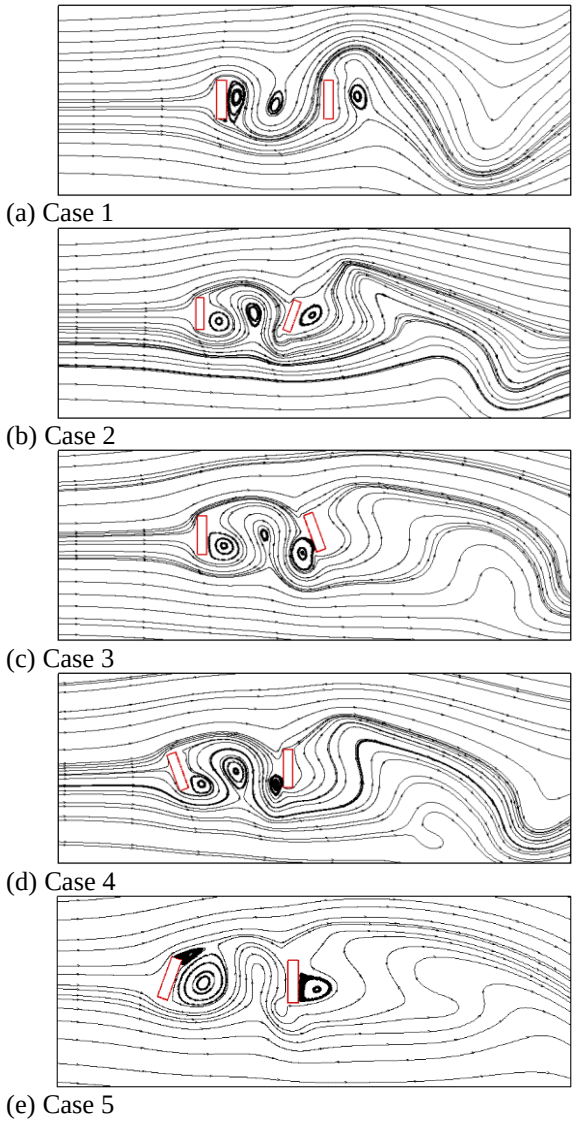

Fig. 8 Instantaneous streamlines at point A, i.e. the lowest peak of the lift curve

sparsely spaced contours, which show a sharp gradient in vorticity. This occurs in Cases 3 and 5, respectively, when the incline causes the distance cylinders to be smaller. When the distance between the two cylinders is left unchanged, as in Cases 1, 2, and 4, widely spaced contours depict areas where the vorticity is more uniform or weaker. Further, for Case 1, the shear layers that were detached from the upstream cylinder rejoin the downstream one, causing a circulation area to develop in the gap. In this case, a vortex core forms in between the cylinders. The formation of a stronger vortex core in between the cylinders, in other cases, is lagged due to the inclination of either cylinder.

The instantaneous streamlines for Cases 1 to 5 are presented in Fig. 8 at the same negative peak point on the C_L time history curve marked with the symbol 'A'. It is seen from Fig. 8a for Case 1 that a stronger vortex behind cylinder 1 is observed. This is associated with more flow blockage and shifting of stagnation point towards the back side of the cylinder. Furthermore, with the inclination of either cylinder, there is still an insufficient the space between the two cylinders. The gap flow is irregular in Figs. 8b to 8e because the upstream split shear layers reattach to the downstream cylinder's leading edge and alternately roll up and down rather than being shed in the space between the cylinders. For Cases 2 to 4, the interaction and combination of the upstream and downstream separated shear-layers result in shedding of vortices in the wake.

3.2. Average Streamlines for Wake Representation

A fluid flows across a cylinder in a certain pattern. The Reynolds number, a dimensionless metric that describes the kind of flow, as well as the flow conditions affects streamline patterns. The flow around the cylinder is normally constant and laminar at low Reynolds numbers. The fluid flows easily around the cylinders in this instance, resulting in a curving streamline that is uniformly spaced and parallel to one another. The streamlined pattern is symmetrical and smooth. Laminar to turbulent flow is observed around the cylinder as the *Re* rises. In this study, the fluid flow for Reynolds numbers 50, 100, 150, and 200 are examined. The streamlines in the aforementioned

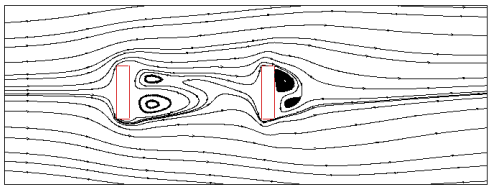

(a) Case 1

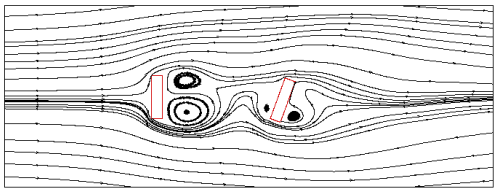

(b) Case 2

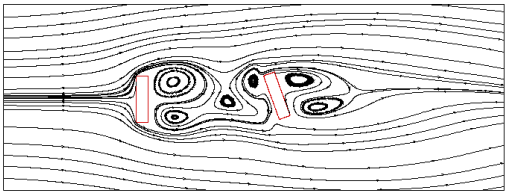

(c) Case 3

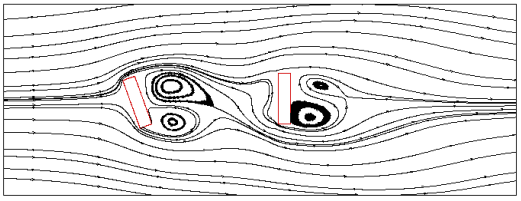

(d) Case 4

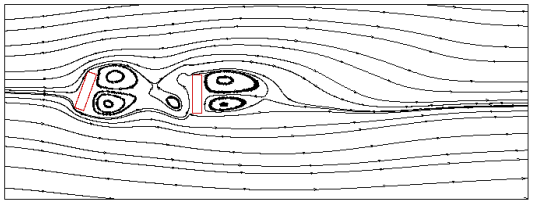

(e) Case 5

Fig. 9 Avearge streamlines behind cylinder 1 and cylinder to represent the wake regime

illustrations demonstrate the fluid's erratic behavior around the rectangular cylinders.

The fluid flows uniformly as it approaches the cylinder from a great distance upstream. At first, the streamlines are straight and parallel to one another. The fluid breaks into two different streams as it approaches the cylinder, one flowing above and one below. Due to the existence of the obstruction, the streamlines swerve around the cylinders. A region of high velocity known as the "stagnation point" is created near the front of the cylinders where the streamlines condense closely. The fluid slows down and changes course at this point. The streamlines then split apart once more as they round the cylinder. The lift force is produced as a result of the pressure differential between the cylinder's upper and lower sides, and it is this lift force that causes the negative vortices to deflect downward. From the five situations i.e. mentioned above and presented in Fig. 9, we saw that vortices are tightly produced when one cylinder is inclined towards the other cylinder. The wake length is reduced with the inclination of either cylinder, *i.e.* for Cases 2 to 4.

3.3. Evolution of Lift Forces

The lift coefficient time history for cylinders 1 and 2 at Re = 150 for Case 1 to Case 5 is represented in Figs. 10a to 10e. It can be indicated that the magnitude of the maximum lift coefficient is highest for Case 1, and the magnitude reduces with either cylinder inclination. Further, for Case 1, both the cylinders represent the same pattern of lift evolution as for the parent single cylinder, as the wake of both cylinders is unaffected by each other. For Case 2 and Case 3, the first cylinder shows a similar pattern, but the second cylinder depicts an entirely different pattern than for the case of the single isolated cylinder. Because of how much gap there is between the two cylinders in this area, the upstream cylinder's wake may totally develop there with only minimal input from the downstream one. When compared to the lift progression of Cases 2 and 3, respectively, the trend for Cases 4 and 5 is the opposite.

3.4. Average Drag Coefficient

The influence of Re on the average drag coefficient for Cases 1 to 5 is represented in Figs. 11a to 11e, respectively. It is seen from Fig. 11 that the maximum drag coefficients for Cylinders 1 and 2 are observed for Case 1. The reduction in the drag is observed with the inclination of either cylinder. Thus it seems to be an effective technique to control the drag for cylinders arranged in tandem fashion. The average drag coefficient monotonously increases with the increase of Reynolds number for Cylinder 1 in Case 1. The steep dwell or hump observe in other cases. It has been claimed that a comparable phenomenon occurs in the cases of square cylinders (Bao et al., 2012) and two tandem circular cylinders (Mizushima and Suehiro 2005).

3.5. Frequency of Vortex Shedding

The amplitude of vortex shedding for Cylinder 1 and Cylinder 2 for Cases 1 to 5 is presented in Fig. 12. It is clearly seen that the magnitude of a frequency significantly reduces for the inclination of either cylinder. Furthermore, an additional small amplitude vortex frequency is also observed for Case 1. In addition, for cylinder inclination in Cases 2 and 3, a high magnitude of vortex shedding frequency is observed for cylinder 2. In a similar manner, alternative peaks are observed for Cases 4 and 5 in comparison with Cases 2 and 3.

3.6. Average Strouhal Number

It can be observed in Fig. 13 that for Case 1, the Strouhal number for both cylinders reduce with the increase of Re. The pattern is similar, as reported by many researchers for the isolated or tandem cylinder arrangement in the open literature. Further, a different pattern is observed for the inclined cylinder cases. The average Strouhal number value first increases up to Re of 100 and then starts decreasing for Cases 2 and 3. The values of the average Strouhal number monotonously increase with the greater of the Re for Cases 4 and 5.

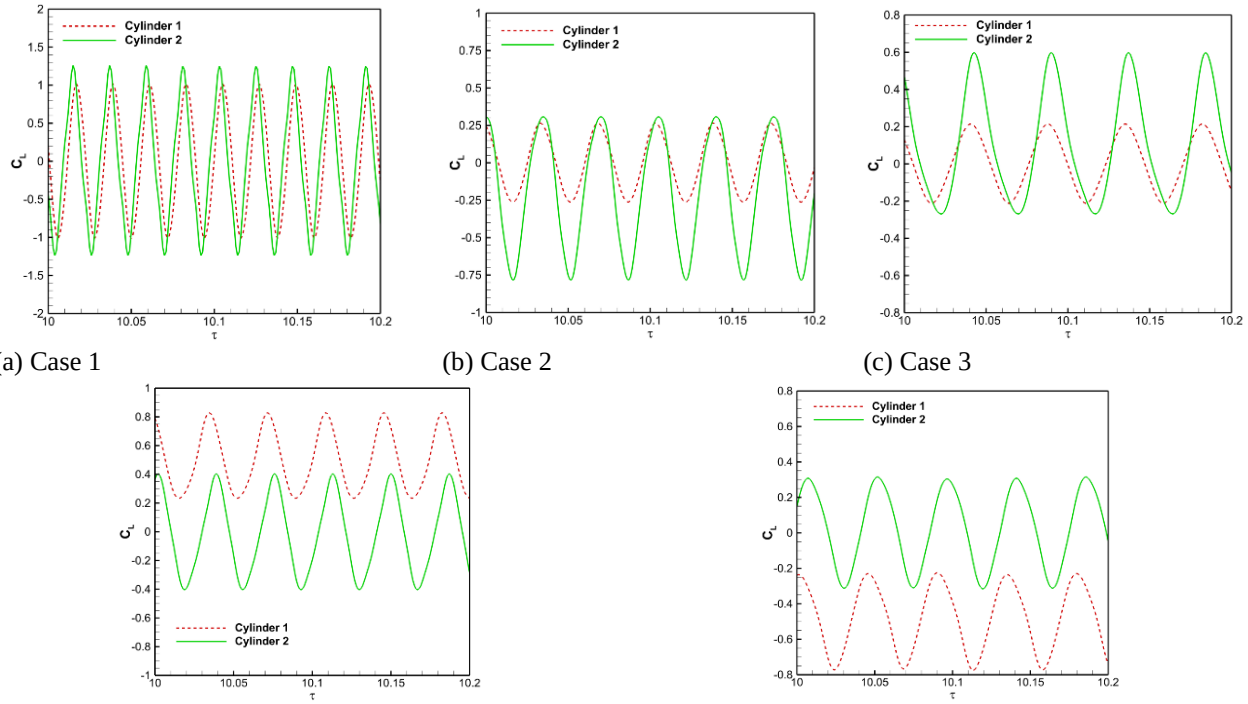

(a) Case 1 (b) Case 2 (c) Case 3

(d) Case 4 (e) Case 5

Fig. 10 Time history of lift forces evolution represented in terms of lift coefficient for cylinder 1 and cylinder at *Re* = 150

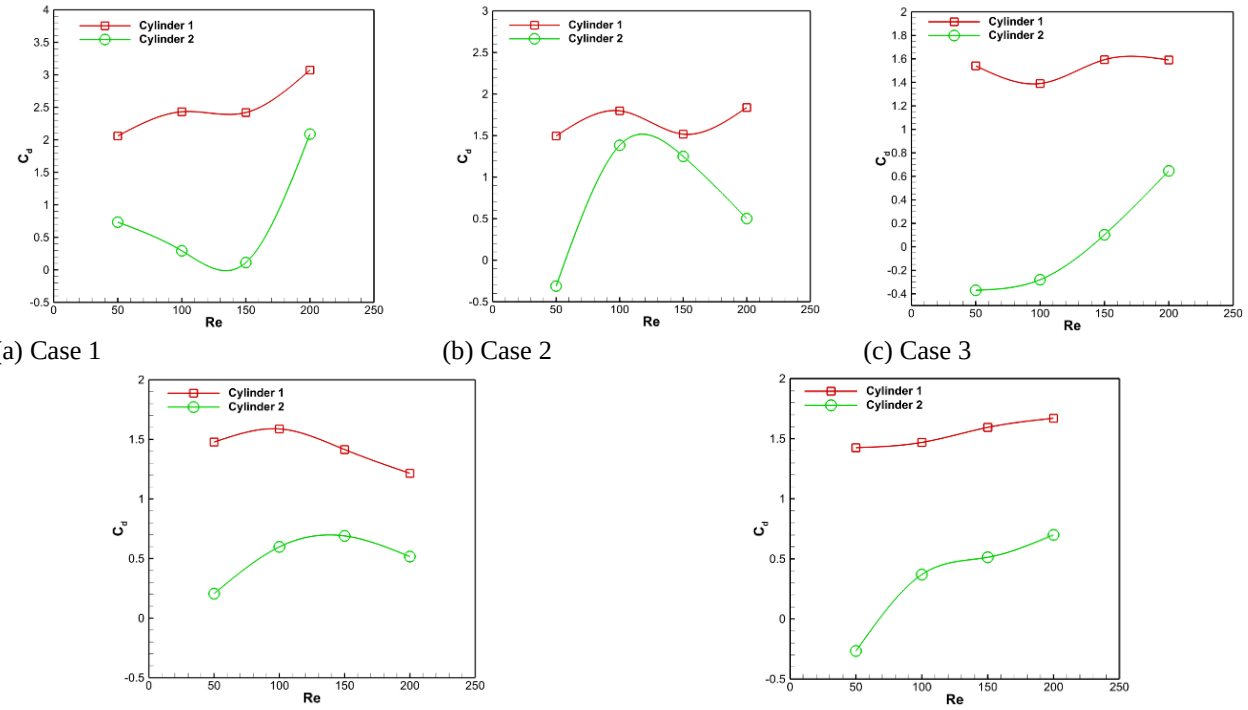

(a) Case 1 (b) Case 2 (c) Case 3

(d) Case 4 (e) Case 5

Fig. 11 Average drag coefficient variation with Reynolds number for cylinder 1 and cylinder

4. CONCLUSIONS

Laminar flow (*Re* = 50–200) around two rectangular cylinders with a fixed aspect ratio of 0.25 and an angle of 20° is studied through a sequence of numerical simulations, both in clockwise and counterclockwise directions. The emphasis is on flow-induced forces and pressures, such as C_D and C_L on the cylinders, as well as fluid properties, including vorticity, vortex shedding, and Strouhal number. An investigation into the impacts of Reynolds number and geometry variations on these variables is the main objective.

- It is discovered by looking at graphs of the lift coefficient that the highest lift for cylinder-1 occurs

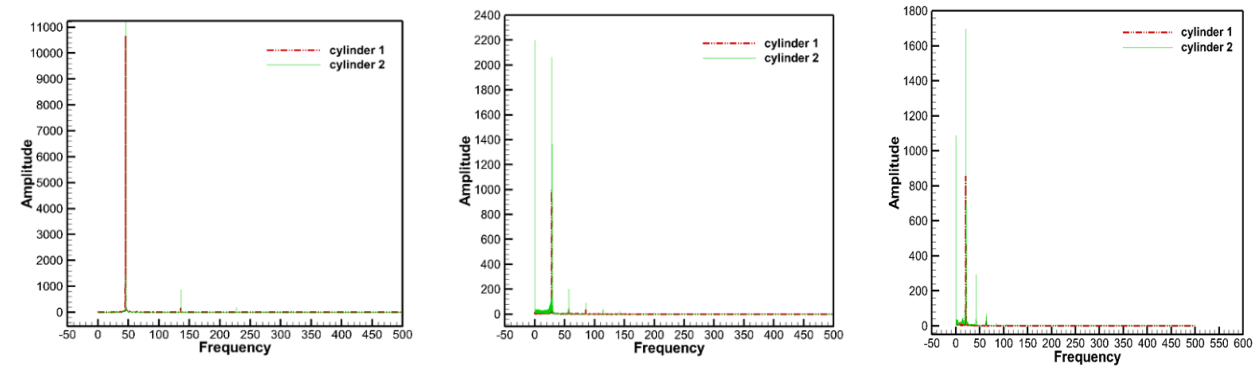

(a) Case 1 (b) Case 2 (c) Case 3

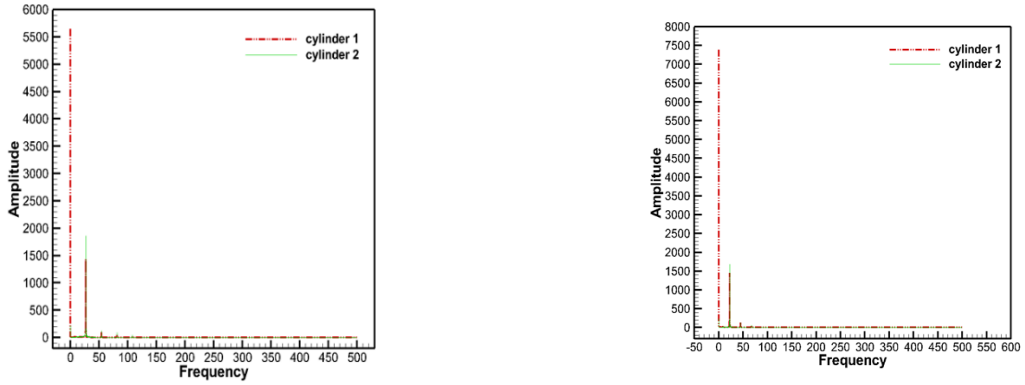

(d) Case 4 (e) Case 5

Fig. 12 Amplitude of vortex shedding at Reynolds number of 150 for cylinder 1 and cylinder

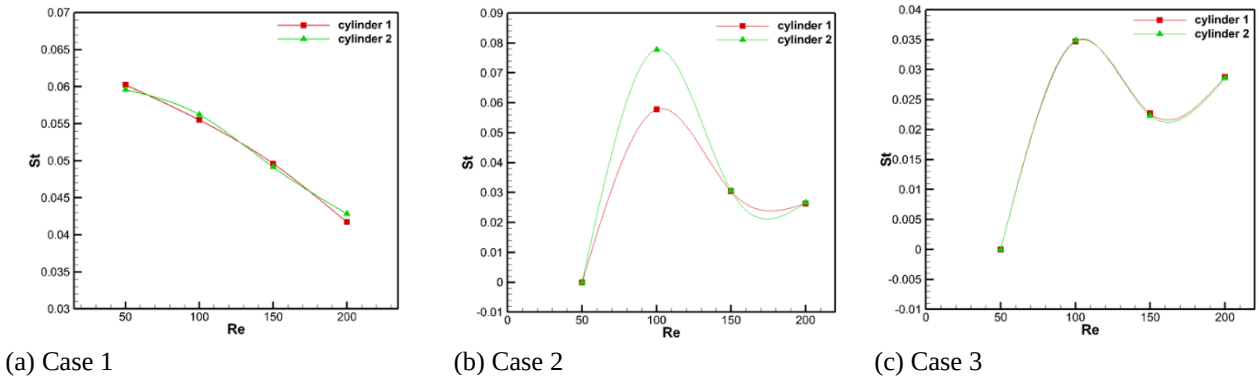

(a) Case 1 (b) Case 2 (c) Case 3

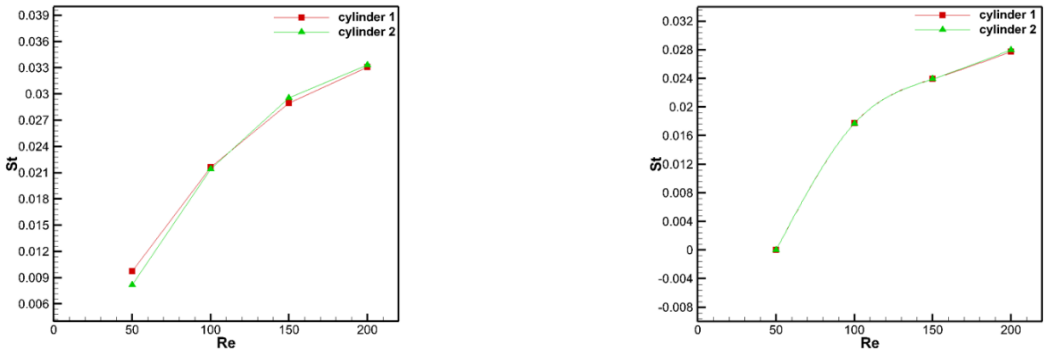

(d) Case 4 (e) Case 5

Fig. 13 Average Strouhal number variation with Reynolds number for cylinder 1 and cylinder

- for Case 4. Further, for Case 1 lift for cylinder 2 is greatest. Additionally, it is discovered that, with the exception of Case 4, cylinder-2 has a larger coefficient of lift than cylinder-1.
- By examining the average drag coefficient graphs for Case 4, it is discovered that cylinder 1 has the lowest drag. For Case 3, drag in cylinder 2 is at its lowest. Additionally, it is discovered that the average drag is always greatest in cylinder one and least in cylinder

two. When the Reynolds number reaches 50 in Cases 2 and 3, the drag coefficient is negative. The average increase in drag for cylinder-1 in all scenarios other than Case 4. The total average drag is at its lowest point in Case 3 at Reynolds number 100 and its highest point in Case 1 at Reynolds number 200.

- For cylinders 1 and 2, the average drag coefficient fluctuation between Reynolds numbers between 50 and 200 varies between 23% and 92%, respectively.
- It is seen from Instantaneous Vorticity graphs that the vorticity is minimal for parallel cylinders. The vorticity is often high when one cylinder is inclined towards the other cylinder.
- Where the cylinders are angled towards one another in Case 3 and Case 5, the average streamlined graphs show a high rate of recirculation and a greater number of densely packed vortices.
- By viewing all of the aforementioned cases aside from Case 4 and Case 5, cylinder 2's amplitude value is at its highest. While the lower frequency is obtained at the point where the highest amplitude is found.
- In Case 1 and Case 3, the minimum and maximum values of Strouhal numbers, respectively, occur at the Reynolds number of 50.

DATA AVAILABILITY

The datasets generated during and/or analyzed during the current study are available from the corresponding author upon reasonable request.

ACKNOWLEDGEMENT

The research work was carried out at Govind Ballabh Pant Institute of Engineering & Technology, Pauri Garhwal, Uttarakhand, India.

CONFLICT OF INTEREST

The authors declared no conflict of interest with anyone for submitting/publishing of this manuscript.

AUTHORS CONTRIBUTION

S. Chamoli: Led the project with conceptualization, methodology, software development, validation, data investigation, resource management, and writing. Also, provided critical input during the review and editing process, created visualizations, supervised the project, and secured funding. **P. Sanwal**: Contributed to the project by refining the conceptualization, implementing methodology, conducting investigations, and curating data. Also, played a role in data visualization. **H. Adhikari**: Assisted in software development, conducted investigations, and contributed to the review and editing of the manuscript. **H. Rana**: Provided formal analysis and contributed to the initial drafts of the manuscript. **P. Pant**: Conducted formal analysis and contributed to the early drafts of the manuscript. **A. Joshi**: Conducted formal analysis and contributed to the early drafts of the manuscript A. **Phila:** Validated the findings, contributed to the initial manuscript drafts, methodology development, and investigations. Also, contributed to the review and editing process and created visualizations. **C. Thianpong**: Played a key role in software development, validation, data investigation, resource management, manuscript creation and secured funding for the project. **S. Eiamsa-ard**: Collaborated in conceptualization and provided supervision.

REFERENCES

Abbasi, W. S., Naheed, A., Ul Islam, S., & Rahman, H. (2021). Investigation of optimum conditions for flow control around two inline square cylinders. *Arabian Journal for Science and Engineering*, *46*, 2845-2864. https://doi.org/10.1007/s13369-020-05303-x

Abdollahpour, M., Gualtieri, P., & Vetsch, D. F., Gualtieri, C. (2023). Numerical study of flow downstream a step with a cylinder Part 2: Effect of a cylinder on the flow over the step. *Fluids*, *8*(2), 60. https://doi.org/10.3390/fluids8020060

Balachandar S., & Parker, S. J. (2002). Onset of vortex shedding in an inline and staggered array of rectangular cylinders. *Physics of Fluids*, *14*(10), 3714-3732. https://doi.org/10.1063/1.1508101

Bao, Y., Wu, Q., & Zhou, D. (2012). Numerical investigation of flow around an inline square cylinder array with different spacing ratios. *Computers & Fluids*, *55*, 118-131. https://doi.org/10.1016/j.compfluid.2011.11.011

Hu, G., Tse, K. T., Kwok, K. C., & Zhang, Y. (2015). Large eddy simulation of flow around an inclined finite square cylinder. *Journal of Wind Engineering and Industrial Aerodynamics*, *146*, 172-184. https://doi.org/10.1016/j.jweia.2015.08.008

Islam, S. U., Manzoor, R., Islam, Z. U., Kalsoom, S., & Ying, Z. C. (2017). A computational study of drag reduction and vortex shedding suppression of flow past a square cylinder in presence of small control cylinders. *AIP Advances*, *7*(4), 045119. https://doi.org/10.1063/1.4982696

Jiang, H., & Cheng, L. (2020). Flow separation around a square cylinder at low to moderate Reynolds numbers. *Physics of Fluids*, *32*(4), 044103. https://doi.org/10.1063/5.0005757

Khademinezhad, T., Talebizadeh, P., & Rahimzadeh, H. (2015). *Numerical study of unsteady flow around a square cylinder in compare with circular cylinder*. 1st National Conference on Fluid Flow, Heat and Mass Transfer, Tehran, Iran. https://www.researchgate.net/publication/272416018

Lekkala, M. R., Latheef, M., Jung, J. H., Coraddu, A., Zhu, H., Srinil, N., & Lee, B. H. (2022). Recent advances in understanding the flow over bluff bodies with different geometries at moderate Reynolds numbers. *Ocean Engineering*, *261*, 11611. https://doi.org/10.1016/j.oceaneng.2022.111611

Liu, C., Gao, Y. Y., Qu, X. C., Wang, B., & Zhang, B. F. (2019). Numerical simulation on flow past two side-by-side inclined circular cylinders at low Reynolds number. *China Ocean Engineering*, *33*(3), 344-355. https://doi.org/10.1007/s13344-019-0033-5

Mashhadi, A., & Sohankar, A. (2022). Two-and three-dimensional simulations of flow and heat transfer around rectangular cylinders. *Computers & Fluids*, *249*, 105689. https://doi.org/10.1016/j.ijmecsci.2020.106264

Mashhadi, A., Sohankar, A., & Alam, M. M. (2021). Flow over rectangular cylinder: Effects of cylinder aspect ratio and Reynolds number. *International Journal of Mechanical Sciences*, *195*, 106264. https://doi.org/10.1016/j.compfluid.2022.105689

Mizushima, J., & Suehiro, N. (2005). Instability and transition of flow past two tandem circular cylinders. *Physics of Fluids*, *17*(10), 104107. https://doi.org/10.1063/1.2104689

Rahman, M. M., Karim, M. M., & Alim, M. A. (2007). Numerical investigation of unsteady flow past a circular cylinder using 2-D finite volume method. *Journal of Naval Architecture and Marine Engineering*, *4*(1), 27-42. https://doi.org/10.1016/j.jfluidstructs.2012.04.006

Rajani, B. N., Kandasamy, A., & Majumdar, S. (2016). LES of flow past circular cylinder at Re= 3900. *Journal of Applied Fluid Mechanics*, *9*(3), 1421-1435. https://doi.org/10.18869/acadpub.jafm.68.228.24178

Sen, S., Mittal, S., & Biswas, G. (2011). Flow past a square cylinder at low Reynolds numbers. *International Journal for Numerical Methods in Fluids*, *67*(9), 1160-1174. https://doi.org/10.1002/fld.2416

Sohankar, A., Norbergb, C., & Davidson, L. (1997). Numerical simulation of unsteady low-Reynolds number flow around rectangular cylinders at incidence. *Journal of Wind Engineering and Industrial Aerodynamics*, *69*, 189-201. https://doi.org/10.1016/S0167-6105(97)00154-2

Sharma, A., & Eswaran, V. (2004). Heat and fluid flow across a square cylinder in the two-dimensional laminar flow regime. *Numerical Heat Transfer, Part A: Applications*, *45*(3), 247-269. https://doi.org/10.1080/10407780490278562

Subburaj, R., & Vengadesan, S. (2019). Flow features for two cylinders arranged in tandem configuration near a free surface. *Journal of Fluids and Structures*, *91*, 102770. https://doi.org/10.1016/j.jfluidstructs.2019.102770

Tahir, N., Abbasi, W. S., Rahman, H., Alrashoud, M., Ghoneim, A., & Alelaiwi, A. (2023). Rectangular cylinder orientation and aspect ratio impact on the onset of vortex shedding. *Mathematics*, *11*(22), 4571. https://doi.org/10.3390/math11224571

Tian, X., Ong, M. C., Yang, J., & Myrhaug, D. (2013). Unsteady RANS simulations of flow around rectangular cylinders with different aspect ratios. *Ocean Engineering*, *58*, 208-216. https://doi.org/10.1016/j.oceaneng.2012.10.013

Tu, J., Zhou, D., Bao, Y., Ma, J., Lu, J., & Han, Z. (2015). Flow-induced vibrations of two circular cylinders in tandem with shear flow at low Reynolds number. *Journal of Fluids and Structures*, *59*, 224-251. https://doi.org/10.1016/j.jfluidstructs.2015.08.012

Wang, Y., Cheng, W., Du, R., Wang, S., & Deng, Y. (2020). Numerical investigation of flow around two tandem identical trapezoidal cylinders. *Mathematical Problems in Engineering*, *2020*, 1-13. https://doi.org/10.1155/2020/3759834

Zhou, C. Y. (2021). The wake and force statistics of flow past tandem rectangles. *Ocean Engineering*, *236*, 109476. https://doi.org/10.1016/j.oceaneng.2021.109476